Cellular and Molecular Life Sciences (2021) 78:757–768
https://doi.org/10.1007/s00018-020-03541-8

ORIGINAL ARTICLE

TET3 controls the expression of the H3K27me3 demethylase *Kdm6b* during neural commitment

Bertille Montibus[1,9] · Jil Cercy[1] · Tristan Bouschet[2] · Amandine Charras[1,10] · Stéphanie Maupetit-Méhouas[1] · David Nury[1] · Céline Gonthier-Guéret[1] · Sabine Chauveau[1] · Nicolas Allegre[1] · Caroline Chariau[3] · Charles C. Hong[4] · Isabelle Vaillant[1] · C. Joana Marques[5,6,7,8] · Franck Court[1] · Philippe Arnaud[1]

Received: 29 November 2019 / Revised: 21 April 2020 / Accepted: 24 April 2020 / Published online: 14 May 2020

Abstract

The acquisition of cell identity is associated with developmentally regulated changes in the cellular histone methylation signatures. For instance, commitment to neural differentiation relies on the tightly controlled gain or loss of H3K27me3, a hallmark of polycomb-mediated transcriptional gene silencing, at specific gene sets. The KDM6B demethylase, which removes H3K27me3 marks at defined promoters and enhancers, is a key factor in neurogenesis. Therefore, to better understand the epigenetic regulation of neural fate acquisition, it is important to determine how *Kdm6b* expression is regulated. Here, we investigated the molecular mechanisms involved in the induction of *Kdm6b* expression upon neural commitment of mouse embryonic stem cells. We found that the increase in *Kdm6b* expression is linked to a rearrangement between two 3D configurations defined by the promoter contact with two different regions in the *Kdm6b* locus. This is associated with changes in 5-hydroxymethylcytosine (5hmC) levels at these two regions, and requires a functional ten-eleven-translocation (TET) 3 protein. Altogether, our data support a model whereby *Kdm6b* induction upon neural commitment relies on an intronic enhancer the activity of which is defined by its TET3-mediated 5-hmC level. This original observation reveals an unexpected interplay between the 5-hmC and H3K27me3 pathways during neural lineage commitment in mammals. It also questions to which extent KDM6B-mediated changes in H3K27me3 level account for the TET-mediated effects on gene expression.

Keywords H3K27me3 · 5-Hydroxymethylcytosine · *Kdm6b* · *Tet3* · Enhancer · Neural stem cells · Neurogenesis

Introduction

Acquisition of cell identity upon differentiation is associated with developmentally regulated changes in the cellular histone methylation signature. This indicates the existence of an epigenetic mechanism to promote the establishment and

Electronic supplementary material The online version of this article (https://doi.org/10.1007/s00018-020-03541-8) contains supplementary material, which is available to authorized users.

✉ Franck Court
franck.court@uca.fr

✉ Philippe Arnaud
philippe.arnaud@uca.fr

1 Université Clermont Auvergne, CNRS, Inserm, GReD, 63000 Clermont-Ferrand, France

2 Institut de Génomique Fonctionnelle (IGF), University of Montpellier, CNRS, INSERM, Montpellier, France

3 Nantes Université, CHU Nantes, SFR Santé, FED4203, Inserm UMS 016, CNRS UMS 3556, 44000 Nantes, France

4 Vanderbilt University School of Medicine Nashville, Nashville, USA

5 Life and Health Sciences Research Institute (ICVS), University of Minho, Campus de Gualtar, Braga, Portugal

6 ICVS/3B's-PT Government Associate Laboratory, Braga, Portugal

7 Department of Genetics, Faculty of Medicine, University of Porto (FMUP), Porto, Portugal

8 i3S-Instituto de Investigação e Inovação em Saúde, Porto, Portugal

9 Present Address: King's College, London, UK

10 Present Address: Department of Women's and Children's Health, Institute of Lifecourse and Medical Sciences, Liverpool University, Liverpool, UK

maintenance of lineage-specific transcriptional patterns. Trimethylation of lysine 27 on histone H3 (H3K27me3), a hallmark of polycomb-mediated transcriptional gene silencing [1], is a central mark in this process. H3K27me3 co-existence with the active trimethylation of lysine 4 on histone H3 (H3K4me3) mark at promoters constitutes the so-called bivalent chromatin that is thought to repress transcription through H3K27me3, while keeping the promoter 'poised' for alternative fates induced by specific developmental cues [2–4]. This scheme, first described in pluripotent stem cells [2, 5, 6], might be important throughout development because bivalent domains have been identified also in multipotent progenitors and differentiated cells [7–13].

The contribution of H3K27me3 dynamics to the fine-tuned regulation of tissue-specific gene expression is best illustrated during neurogenesis. Commitment towards the neural lineage as well as the fate of neural progenitors and the specification of neuronal subtypes are regulated by polycomb group proteins [14–17]. These processes are associated with H3K27me3 gain or loss at specific sets of genes during neurogenesis. For instance, Albert et al. recently demonstrated at the *Eomes* locus that inhibition by genome editing of the transient decrease of H3K27me3 normally observed at this gene promoter in the developing cortex leads to lower expression of this transcription factor and altered neocortex development [13].

KDM6B is a key factor in the temporally regulated demethylation of H3K27me3. This JmjC-domain-containing protein is an H3K27me3-specific demethylase [18, 19] that is essential for neurogenesis [20]. Specifically, KDM6B critical role in embryonic stem (ES) cell commitment toward the neural lineage and in the activation of the lifelong neurogenic program relies on its capacity to catalyze H3K27me3 removal at gene promoters and enhancers [21–23].

Therefore, to better understand the epigenetic regulation of neural fate acquisition, it is important to determine how *Kdm6b* expression is regulated. Here, we investigated the molecular mechanisms involved in the control of *Kdm6b* expression upon mouse ES cell commitment towards neural lineages. Altogether, our data revealed a model; whereby, *Kdm6b* induction upon neural commitment relies on an intronic enhancer the activity of which is defined by its ten-eleven-translocation 3 (TET3)-mediated 5-hmC level.

Materials and methods

Cell culture and ES cell differentiation

Wildtype ES cells were derived from blastocysts obtained from crosses between C57BL/J (B) and JF1 (J) mice, and were maintained in gelatin-coated dishes with ESGRO complete plus medium (Millipore, SF001-500P) that contains LIF, BMP4, and a GSK3-β inhibitor. In vitro corticogenesis was performed as described previously [24], except that ES cells were plated on Matrigel-coated dishes (human ES cell-qualified matrix, Corning), and that Defined Default Medium was supplemented with B27 (without vitamin A, Gibco) to improve cell survival, and with 1 µM dorsomorphin homolog 1 (DMH1) (purified by C.C.H) to promote neurogenesis [25]. Using this protocol, neural precursors (NP) cells are the main cell population after 12 days (D12) of in vitro corticogenesis [24].

Expression analysis

Total RNA was extracted using TRIzol Reagent (Life Technologies, 15596018). After treatment with RNase-free DNase I (Life Technologies, 180868-015), first-strand cDNA was generated by reverse transcription with Superscript-IV (Life Technologies, 18090050) using random primers and 500 ng of RNA. *Kdm6bos* antisense RNA expression was analyzed by strand-specific reverse transcription. cDNA was then amplified by real-time PCR with a SYBR Green mixture (Roche) using a LightCycler R 480II (Roche) apparatus. The relative expression level was quantified with the 2-dCt method that gives the fold change variation in gene expression normalized to the geometrical mean of the expression of the housekeeping genes *Gapdh*, *Tbp*, and *Gus* (for *Kdm6b*, *Tet1*, *Tet2*, *Tet3*, *Pou5f1*, *Nestin*, and *Pax6* expression analysis during corticogenesis), *Rpl30* and *Ppia* (for *Tet3* expression analysis in NP cells derived from ES cells incubated with retinoic acid), or *Gapdh*, *Tbp*, *Rpl30*, and *Ppia* (for *Kdm6a* and *Kdm6b* expression analysis in NP cells derived from ES cells incubated with retinoic acid). For *Kdm6bos*, gene expression was normalized to the geometrical mean of the strand-specific expression of the housekeeping genes *Rpl30, Ppia,* and *Rps17*. Each analysis was performed at least in triplicate. Details on the primers are in Supplementary Table 1.

Chromatin immunoprecipitation

Anti-H3K9ac (Millipore 06-942), -H3K4me3 (Diagenode 03-050), and -H3K27me3 (Millipore 07-449) antibodies were used for chromatin immunoprecipitation (ChIP) of native chromatin (N-ChIP) isolated from ES and NP cells (D12 of in vitro corticogenesis) [12].

An anti-TET3 antibody (polyclonal ABE290 Millipore), which targets the three TET3 isoforms (TET3FL, TET3s, TET3o; [26]), anti-H3K4me1 (Millipore, 07-436) and an anti-H3K27ac (Abcam Ab4729) antibody were used to assess their enrichment by ChIP of cross-linked chromatin (X-ChIP) isolated from ES and NP cells (D12).

Briefly, cells were resuspended in PBS (1 million of cells per ChIP) and fixed in 1% formaldehyde (Sigma-Aldrich, F8775) by shaking at 700 rpm at room temperature for 6 min. The subsequent steps were performed using the Zymo-Spin ChIP Kit (Zymo Research, D5210) according to the manufacturer's instructions. Chromatin was sonicated on a Bioruptor™ Next Gen for 4 × 11 cycles (30 s on/30 s off) at 4 °C.

Input and antibody-bound fractions were quantified by real-time PCR amplification with the SYBR Green mixture (Roche) using a LightCycler 480II (Roche) instrument. Background precipitation levels were determined by performing mock precipitations with a non-specific IgG antiserum (Sigma C-2288), and were only a fraction of the precipitation levels obtained with the specific antibodies. The bound/input ratios were calculated and normalized to the precipitation level at the *Rpl30* promoter for anti-H3K9ac and -H3K4me3 ChIPs, at the *Hoxa3* promoter for anti-H3K27me3 ChIPs, and at the *IAP* promoter for anti-H3K9me3 ChIPs. Normalization was not used for analysis of TET3, H3K4me1, and H3K27ac enrichment. The used primers are described in Supplementary Table 1.

Gene-specific bisulfite sequencing and combined bisulfite restriction analysis

Bisulfite conversion, PCR amplification, digestion for combined bisulfite restriction analysis (COBRA), cloning, and sequencing were performed as previously described [27]. Briefly, following bisulfite treatment, restriction sites are created (or maintained) only if their recognition site corresponds to a methylated cytosine in the native DNA (therefore, unconverted in the PCR product). For example, TCGA in the native sequence will become TTGA if the first cytosine is unmethylated, or will remain TCGA, if it is methylated. In this last case, the *Taq*1 site is maintained. Such sites can be found frequently in PCR products. Thus, digestion with *Taq*1 will indicate the 'methylation pattern' of the molecule population in the PCR products.

Details on the primers are in Supplementary Table 1.

5hmC detection

5hmC was analyzed using the EpiMark® 5-hmC and 5-mCAnalysis Kit (E33175, New England Biolabs) according to the manufacturer's instructions. Briefly, genomic DNA was incubated with the T4-β-glucosyltransferase that protects against *Msp*I digestion (CCGG) by adding a glucose moiety specifically to 5-hydroxymethylcytosine residues. The 5hmC levels were then determined by quantifying the *Msp*I-resistant fraction in each sample by qPCR using primers designed around the analyzed *Msp*I sites. The data were normalized to the amplification of the same region in the original DNA input. The obtained values were corrected relative to the basal rate of *Msp*I digestion in untreated DNA. The primer sequences are in Supplementary Table 1.

Tet3 knockdown

Tet3 knockdown was performed as described in Ref. [28]. Briefly, shRNA-mir cassettes for the *Tet3* gene were amplified from pSM2 retroviral vectors containing the shRNAmir sequences (Open Biosystems) and cloned into the p2Lox vector using *Hind*II and *Not*I restriction sites. Then, to stably integrate these shRNAs (p2Lox constructs) were transfected into the A2lox.cre ES cells (derived from the E14 male cell line from the mouse strain 129P2/OlaHsd) [29] that express Cre after the addition of doxycycline (0.5 µg/ml) to the medium one day before transfection. ES cells were then transfected using Lipofectamine 2000 (Invitrogen) at a concentration of 5×10^5 cells/ml. One day after transfection, selection medium containing geneticin (G418, Melford—300 µg/ml active concentration) was added to the cells for 10 days. After selection, ES cell clones containing the shRNAmir were expanded in ES complete medium.

Neural differentiation of A2lox.cre ES cells was performed by incubation with retinoic acid from day 4 to day 8 of culture, resulting in a homogeneous NP population of PAX6-positive radial glial cells, as previously described in Ref. [30]. For shRNA expression after differentiation, doxycycline (2 µg/ml) was added to the medium for 5 days, and then cells were trypsinized and pellets stored at − 80 °C until analysis.

Western blotting

Proteins from ES and NP cell (D12) pellets were extracted with RIPA buffer containing Protease Inhibitor Cocktails (Roche, 04693159,001) (25 µl of buffer for 1 million cells). The lysate protein content was determined with the Bradford assay. Equal amounts of proteins (50 µg) were separated by SDS–PAGE, and then transferred to PVDF membranes (Bio-Rad). After membrane blocking, specific antibodies against KDM6B (Abcam Ab84200, rabbit, 1/500) and GAPDH (Sigma Ab2302, chicken, 1/10,000) were added overnight. Next, membranes were incubated with peroxidase-conjugated secondary antibodies against rabbit (Abliance Bl2407, 1/500) and chicken (Santa Cruz sc2428, 1/10,000) for 2 h. Finally, interactions were detected using the Clarity

Western ECL substrate kit (Bio-Rad 1705060) according to the supplier, and the Chemidoc MP Imaging System apparatus (Bio-Rad).

Chromosome conformation capture (3C) analysis

The chromatin conformation capture (3C) protocol was performed as previously described [31] with minor modifications. Nuclei from ES and NP cells were extracted according the protocol described in Ref. [32], and purified on sucrose gradient. Between 1 and 5 M of formaldehyde-fixed nuclei were used for these experiments, and a total of 600 U of *Dpn*II enzyme was used for chromatin digestion. Then, the 3C template was digested with 40U of *Nla*III. Standards curves for qPCR were generated using BAC RP23-167O7. Primer sequences are in Supplementary Table 1.

Race-PCR

Race analyses were performed with Gene Racer™ (Invitrogen, L1500-01) according to the manufacturer's instructions.

Raw data from ChIP-seqData mining

experiments in ES and NP cells were retrieved from GEO DataSets or from the Encode project (the accession numbers for the data are indicated in Supplemental Table 2). Reads were aligned to the mm9 genome using bowtie2 (version 2.3.4.3). Alignments with a MAPQ lower than 30 were filtered out using samtools (version 1.9). Coverage tracks of these alignments were produced with bamCoverage using RPKM normalization, a read extension of 200 pb, the ignoreDuplicates option, and a bin size of 20 pb. These coverage tracks were loaded on the UCSC genome browser for visualization.

Several high-throughput alignments were obtained from the UCSC genome browser. The ChiP-seq alignments for H3K27ac, H3K4me1, and H3K4me3 in cortex samples were from the LICR histone track, DNase experiments in mouse ES cells and in mouse brain were from the UW DNaseI HS track, and DNA methylation data (WGBS and RRBS) were from the HUB DNA Methylation of UCSC and the Stadler 2011 and Booth 2012 tracks, respectively. BedGraph tracks of the GRO-seq data for ES cells were retrieved from the GEO dataset GSE48895. The Pearson's correlation coefficients for *Kdm6b* and *Tet* expression data were obtained using the pseudo-counts associated with the GSE58523 dataset [33].

Statistical analysis

Statistical analysis was performed using GraphPad Prism 7.02, or R3.6.1. The number of independent experiments and the name of the statistical test used for each comparison are indicated in the legends.

Results

Kdm6b is upregulated upon neural commitment

The canonical mouse *Kdm6b* gene is about 15 kb-long and is located on chromosome 11. It contains 23 exons, including three that are untranslated and located in the 5′ part (Fig. 1a). To determine its regulation upon neural commitment we chose an established in vitro protocol that uses ES cells to recapitulate the sequential steps of mouse in vivo corticogenesis [24, 33]. We focused on the first 12 days of in vitro corticogenesis. During this period, ES cells differentiated mainly into NP cells, as indicated by the marked downregulation of the pluripotency marker *Pou5f1* and the upregulation of the neural progenitor markers *Nestin* and *Pax6* (Supplementary Fig. 1a). Concomitantly, *Kdm6b* expression level increased by more than five times (Fig. 1b and Supplementary Fig. 1b), leading to a marked increase in its protein level in NP cells at day 12 (D12) (Fig. 1c). Hereafter, D12 of in vitro corticogenesis will be referred to as "NP cell stage".

To determine the molecular bases of this upregulation, we first wanted to delineate the *Kdm6b* promoter region(s) in ES cells and after their differentiation into NP cells using Race-PCR. This approach revealed that besides the documented transcription start site (TSS) in exon 1, a large subset of *Kdm6b* transcripts initiated from a CpG island (CGI) located in intron 1 and referred to as CGI2 (Fig. 1a, Supplementary Fig. 1c). CGI2 emerged as one of the main *Kdm6b* promoters. This observation was further supported by publicly available GRO-seq data from ES cells showing a cluster of initiation sites along CGI2 (Supplementary Fig. 1d). Accordingly, and unlike CGI1, this region displayed a dynamic histone modification profile between ES and NP cells. In ES cells, H3K4me3 and also H3K27me3, although at a lower level, were enriched at CGI2, constituting a "weak" bivalent domain. This signature was lost in NP cells due to the H3K27me3 decrease and the gain in H3K4me3 and acetylation of lysine 9 on histone H3 (H3K9ac), which in combination generally mark active promoters (Fig. 1d). DNA at both CGIs remained unmethylated throughout the experiment (Supplementary Fig. 1d).

These data indicate that *Kdm6b* upregulation upon neural commitment is associated with changes in the histone mark signature at CGI2, one of its main promoters.

Dynamic 3D conformation changes at the *Kdm6b* locus upon neural commitment

To identify putative regulatory regions, we looked for regions that physically interact with CGI2 in ES and NP

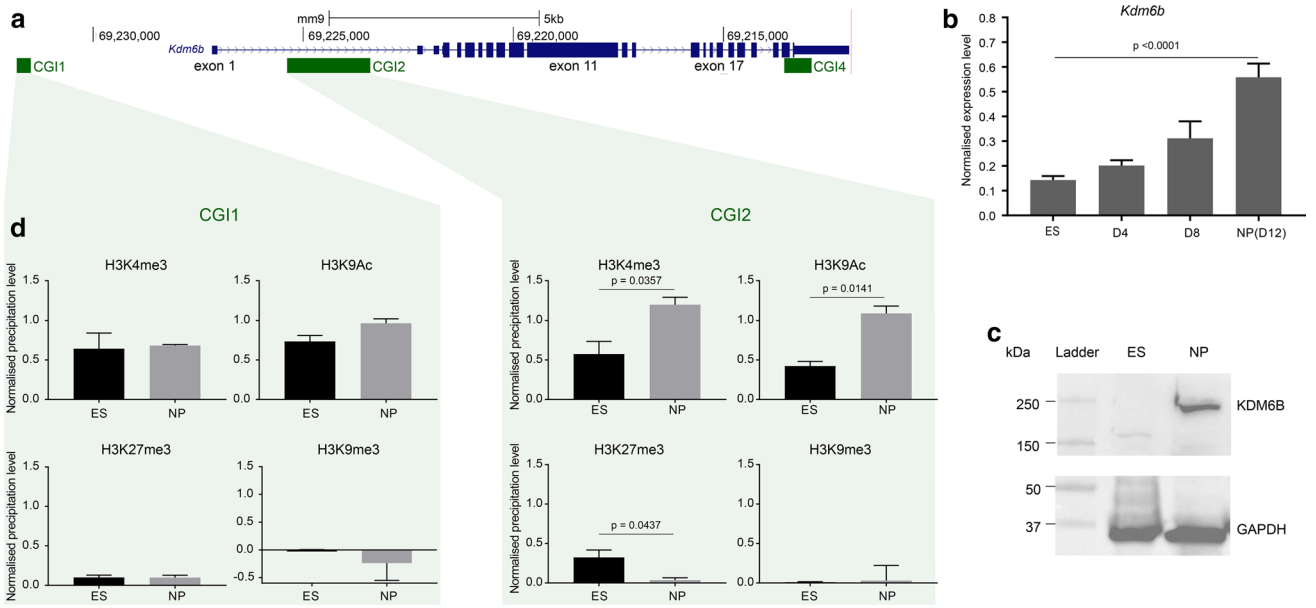

Fig. 1 *Kdm6b* is upregulated upon neural commitment. **a** Map of the mouse *Kdm6b* locus showing the CpG islands (CGI) and exons as described in the UCSC Genome Browser. Positions are given according to the mm9 assembly. **b** *Kdm6b* expression level in ES cells ($n=6$) and at day 4 (D4; $n=3$), D8 ($n=3$), and D12 (NP cell stage; $n=6$) of in vitro corticogenesis. The expression was assessed with primers located on exons 5 and 6. Statistical significance was determined by one-way ANOVA (comparison of each differentiation point with ES cells). **c** KDM6B protein level evaluated by western blotting in ES and NP cells (D12). **d** ChIP analysis of H3K9ac, H3K4me3, H3K27me3, and H3K9me3 enrichment at CGI1 and CGI2 in ES ($n=3$) and NP ($n=3$) cells. The precipitation level was normalized to that obtained at the *Rpl30* (for H3K4me3 and H3K9ac), *HoxA3* (for H3K27me3), and IAP (for H3K9me3) promoters. Statistical significance was determined with the unpaired *t* test (p values in the figure). The data are presented as the mean ± SEM

cells by using the 3C approach. As such contacts are strongly favored between genomic regions that belong to the same topologically associating domain (TAD), we first checked using publicly available data [34, 35] that the *Kdm6b* locus was not close to a TAD boundary (Supplementary Fig. 2a). Then, we tested whether 15 regions distributed along a 22 kb window that includes the *Kdm6b* locus could interact with CGI2. We found that in ES cells, CGI2 mainly interacted with exon 11 and to a lesser extent with exons 17–21. Conversely, at the NP cell stage, the CGI2 interaction with exon 11 became restricted to the 5′ part of the exon, whilst the interaction between exons 17–21 and CGI2 was markedly increased (Fig. 2a). In human *KDM6B*, the region encompassed by exons 17–21 contains a CGI not described in the mouse genome (Supplementary Fig. 2b). However, we detected the presence of a "weak" CGI between exon 17 and 18 in the mouse gene that we called CGI3. CGI3 met all criteria for a CGI (GC content ≥ 50% and ratio of observed to expected number of CG dinucleotides > 0.6) but one (i.e., size > 200 bp), because it is 196 bp in size. Reciprocally, when CGI3 was used as anchor, this region mainly interacted with CGI2 in NP cells (Fig. 2a, right panels).

As supported also by GRO-seq data in ES cells (Supplementary Fig. 2d), CGI3 contained the documented transcriptional start site of *Kdm6bos*, and thus was the promoter for this *Kdm6b* small antisense transcript (Fig. 2b). This non-coding transcript was poorly expressed in ES and NP cells (Supplementary Fig. 2c). Data mining revealed that a DNase I hypersensitive site was located within CGI3 in ES cells and whole brain. These two features, generally found at enhancers, suggest that CGI3 could be a regulatory region. Data mining also showed a marked enrichment for the boundary protein CTCF at CGI3 in ES and NP cells (Fig. 2b). However, neither CGI3 nor exon 11 displayed the canonical chromatin signature generally observed at enhancers (Fig. 2c). ChIP analyses in ES and NP cells associated with data mining showed H3K4me1 enrichment at CGI3. However, this enrichment was not specific to that region, but rather present throughout the whole locus (Fig. 2c, Supplementary Fig. 2d). In addition, H3K27ac, which is indicative of an active enhancer and promoter, was enriched in

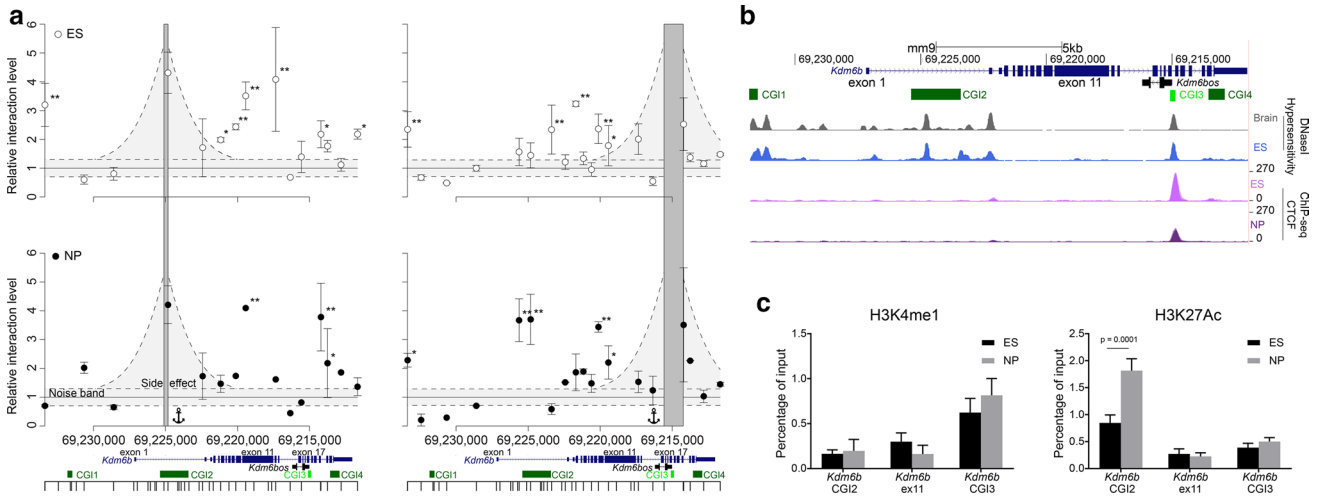

Fig. 2 3D conformation of the *Kdm6b* locus in ES and NP cells. **a** 3C data quantification at the *Kdmb6* locus. The left panels show the relative interaction frequencies between CGI2 (the anchor region) and the 15 tested sites along the locus, in ES cells (white circles) and NP cells (black circles). Four independent experiments were performed. Data points represent the mean ± SD of those that have provided a detectable quantification signal. The right panels show the relative interaction frequencies using the "weak" CGI3 area as anchor region. The noise band was defined using the basal interaction level (BIL [31]) ± 1 standard deviation (SD) of BIL (gray area); significant interactions were identified when the relative interaction level was higher than the BIL + 3 SD for (*) or 4 SD (**). **b** Data mining of DNase I hypersensitivity and CTCF recruitment at the *Kdm6b* locus in ES cells, whole brain, and NP cells. The Ensembl transcript ENSMUSG00000085178 (named *Kdm6bos* in the mm10 assembly) initiates from CGI3. **c** ChIP analysis of H3K4me1 (left panel) and H3K27ac (right panel) at CGI2, exon 11, and CGI3 in ES ($n = 4$) and NP cells ($n = 4$). Statistical significance was determined by two-way ANOVA (p values in the figure). The data are presented as the mean ± SEM

the 5′ part of the locus that included CGI2, but was at basal level at exon 11 and CGI3, in both ES and NP cells (Fig. 2c, Supplementary Fig. 2d).

In conclusion, these approaches suggest that CGI3 is a putative regulatory region, despite the absence of a canonical enhancer chromatin signature.

5hmC enrichment switches from exon 11 to CGI3 during differentiation of ES cells into NP cells

Due to the relative high level of 5-hydroxymethylation (5hmC) in ES cells and in the central nervous system [36, 37] and its enrichment at regulatory regions including enhancers [38, 39], we next investigated the 5mC/5hmC profile at exon 11 and CGI3 of *Kdmb6*. Bisulfite analysis, supported by publicly available whole-genome bisulfite sequencing (WGBS) data, showed that like CGI1 and CGI2, CGI3, and CGI4 (a CGI located in the last exon of *Kdmb6*) were not methylated in ES cells. In NP cells, CGI3 and CGI4 showed a limited gain of methylation, while CGI1 and CGI2 remained unmethylated. In contrast, we observed a marked methylation gain at exon 11 that was partially methylated in ES cells, and fully methylated in NP cells (Fig. 3a,b and Supplementary Fig. 1d).

As bisulfite sequencing cannot distinguish between 5mC and 5hmC, we wanted to know whether the low level of DNA methylation at exon 11, CGI3 and CGI4 could be explained by 5hmC deposition. To this aim, first we analyzed publicly available oxidative reduced representation bisulfite sequencing (oxRRBS) data for ES cells. In this approach, the level of 5mC and 5hmC are obtained by comparing the data generated using the same material by reduced representation bisulfite sequencing (RRBS), which detects both modifications, and by oxRRBS, which only detects 5mC [40]. This analysis highlighted 5hmC enrichment at exon 11 in ES cells (Fig. 3a). Then, we took advantage of the fact that following glucosylation, the C(5hm)CGG site becomes insensitive to *Msp*I. Thus, analyses of glucosylated and untreated DNA from ES and NP cells allowed us to evaluate 5hmC level at nine *Msp*I-containing regions throughout the *Kdm6b* locus. This approach confirmed 5hmC enrichment at exon 11 (covered by three sites) in ES cells, and indicated that 5hmC level was decreased in NP cells, particularly in its 3′ part. We observed the same dynamics at the region located immediately upstream of CGI3. Conversely, at the region located immediately downstream of CGI3 and within CGI4, 5hmC increased from the ES to the NP cell stage (Fig. 3c), suggesting again that

the limited methylation gain observed at CGI3 and CGI4 by classic bisulfite sequencing (Fig. 3a, b) was, at least in part, a 5hmC gain.

These data revealed that at exon 11 and in the CGI3–CGI4 area of the *Kdm6b* locus, 5hmC level changes during ES cell differentiation into NP cells and parallels the changes in CGI2 interactions.

TET3 is required for *Kdm6b* upregulation

Deposition of 5hmC is catalyzed by the TET methylcytosine oxidase family that includes three members in mammals (TET1, TET2, and TET3). In agreement with the literature [41], we observed strong expression of *Tet1* and *Tet2,* but not of *Tet3* in ES cells. In addition, as documented in the developing brain [39], all three TETs were expressed during in vitro corticogenesis, although at very low level for *Tet1* (Fig. 4a). *b* is upregulated u We found that only *Tet3* expression was significantly correlated with *Kdm6b* expression ($R = 0.8$) (Fig. 4b).

Moreover, ChIP analyses showed that at the NP cell stage, TET3 was recruited at the *Kdm6b* locus, particularly at CGI3 and CGI4, precisely where we observed a 5hmC gain (Fig. 4c). Finally, shRNA-mediated knockdown of *Tet3* in NP cells derived from ES cells using a retinoic acid-based protocol showed that *Tet3* downregulation was associated with reduced *Kdm6b* expression, without any effect on *Kdm6a*, the other H3K27me3 demethylase (Fig. 4d). When combined, these observations suggest that *Kdm6b* upregulation during neural commitment is dependent on TET3 recruitment to CGI3, its putative regulatory region.

Discussion

Taken together, our data suggest that TET3 and 5hmC dynamics contribute to the control of *Kdm6b* expression during neural commitment.

We evidenced that *Kdm6b* shows two main 3D configurations during in vitro corticogenesis. In ES cells, where *Kdm6b* expression is low, the predominant 3D configuration was defined by the contact between one of its main promoters (CGI2) and exon 11. The second 3D configuration is mainly observed in NP cells, and is characterized by the contact between the promoter and CGI3, a previously uncharacterized intragenic CGI that displays several enhancer features. This promoter–enhancer contact might explain *Kdm6b* upregulation in NP cells. Moreover, we found that the change between 3D configurations correlates with a switch in 5hmC enrichment from exon 11 in ES cells to the CGI3 area (up to CGI4) in NP cells.

The 5hmC gain at the CGI3 area in NP cells is reminiscent of what observed at tissue-specific enhancers during cardiomyocyte and hematopoietic cell differentiation, for instance [42, 43]. This event might constitute an early step in the enhancer activation that could facilitate chromatin opening and the recruitment of pioneer transcription factors [38, 44]. The 5hmC enrichment at exon 11 upon differentiation suggests that 5hmC deposition might also have a more structural function, by stabilizing the contact between two distal genomic regions. In this scheme, 5hmC enrichment at exon 11, likely controlled by TET1 or TET2, would favor its unproductive interaction with the *Kdm6b* promoter in ES cells. The low *Kdm6b* expression observed at this stage could be explained by contacts between CGI2 and CGI3 in a subset of cells. Upon differentiation, 5mC gain at exon 11, possibly due to the decrease in TET1/2 levels, associated with TET3-mediated 5hmC gain at the CGI3 area would favor CGI2–CGI3 interactions. This could be further promoted by CTCF binding at CGI3. Indeed, it has been recently shown that CTCF reduces cell-to-cell variations by stimulating enhancer–promoter activity [45]. Therefore, CTCF could act upstream or conjointly with 5hmC to stabilize the interaction between CGI2 and CGI3 and ensure robust *Kdm6b* expression in NP cells (Fig. 5).

Besides providing information on how *Kdm6b* expression is regulated, our study unravels the tight interplay between the 5hmC and H3K27me3 pathways during neural commitment. These two key epigenetic pathways are crucial for neural development. For instance, 5hmC is very abundant in brain compared with other organs. Moreover, TET3 plays a critical role in neurogenesis [39, 46]. Our original observation raises the question of whether and to which extent KDM6B-mediated changes in H3K27me3 level can account for TET-mediated effects on gene expression during neural commitment. Functional studies on TETs in ES cells indirectly support such interplay with other epigenetic programs for regulating gene expression. In these studies, there is little correlation between changes in DNA methylation at the promoter and changes in gene expression following TET depletion [47–51]. For instance, in embryoid bodies differentiated from TET triple-knockout ES cells, about 70% of genes with reduced expression do not show any DNA methylation defect [52], suggesting that TET could indirectly control a subset of these genes. TET3-mediated control of *Kdm6b* might also be part of a more general developmental program. Indeed, TET1 is involved in the

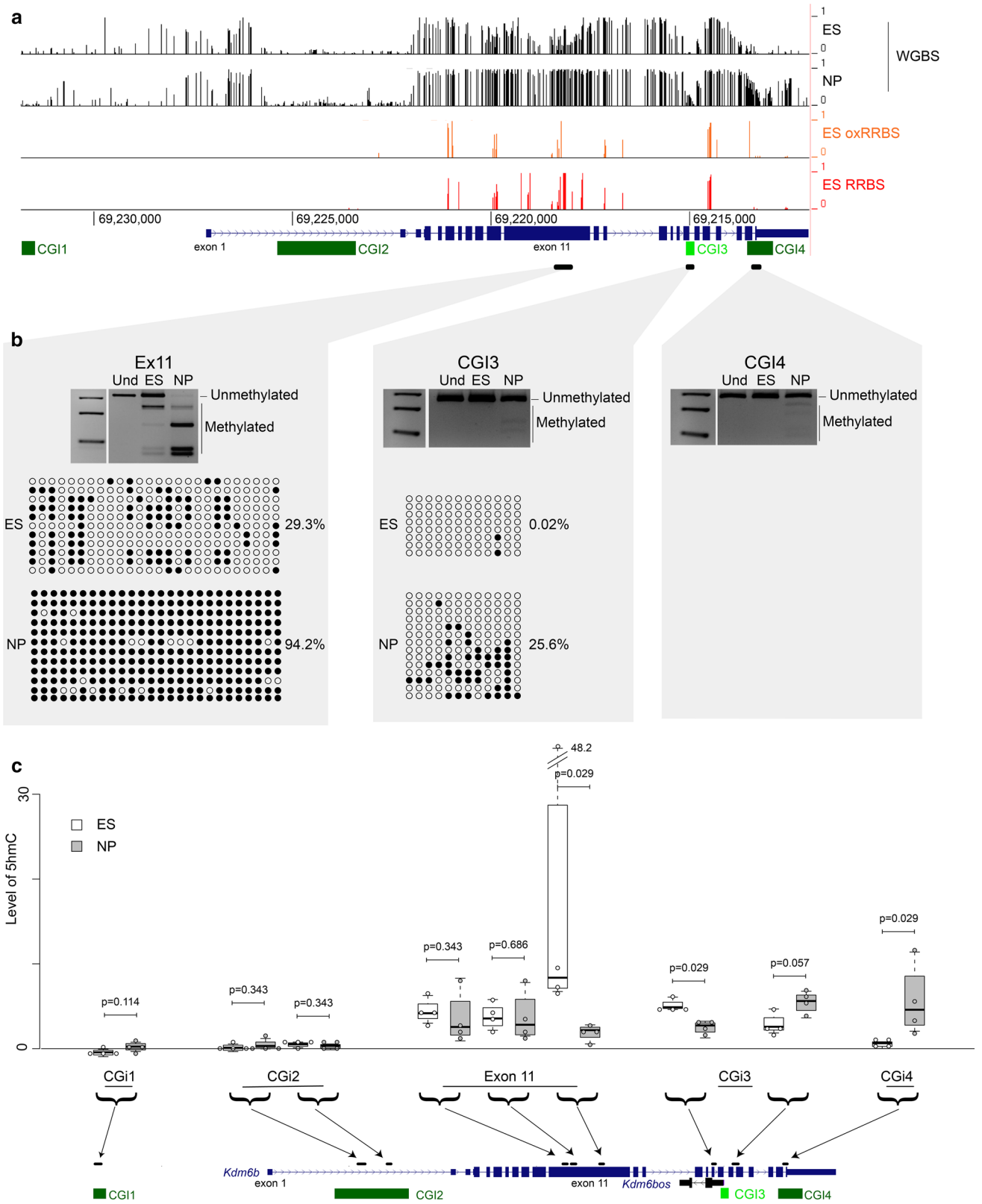
a
ES
NP
WGBS
ES oxRRBS
ES RRBS
69,230,000
69,225,000
69,220,000
69,215,000
CGI1
exon 1
CGI2
exon 11
CGI3
CGI4
b
Ex11
CGI3
CGI4
Und ES NP
Unmethylated
Methylated
ES
NP
29.3%
94.2%
0.02%
25.6%
c
Level of 5hmC
ES
NP
48.2
p=0.029
p=0.114
p=0.343
p=0.343
p=0.343
p=0.686
p=0.029
p=0.057
p=0.029
CGi1
CGi2
Exon 11
CGi3
CGi4
Kdm6b
exon 1
exon 11
Kdm6bos
CGI1
CGI2
CGI3
CGI4

◂**Fig. 3** Changes in 5hmc level at the *Kdm6b* locus during ES cell differentiation into NP cells. **a** Data mining of 5mC by WGBS (ES and NP cells) and of 5hmC by comparing the RRBS and oxRRBS datasets (ES cells) at the *Kdm6b* locus. **b** Bisulfite-based DNA methylation analyses at exon 11, CGI3, and CGI4 by COBRA and/or sequencing in ES and NP cells. For each sequenced region, the methylation patterns are symbolized by lollipops (black: methylated CpG; white: unmethylated CpG). For each region, PCR analysis was repeated using 3 independent samples for ES and for NP cells that gave similar results. The results of one representative experiment are shown. **c** 5hmC distribution along the *Kdm6b* locus in ES (white boxes; $n=4$) and NP cells (gray boxes; $n=4$), respectively. Levels of 5hmC are given as the level of the *MspI*-resistant fraction at each analyzed region. Statistical significance was determined with the Mann–Whitney test (p values in the figure). The data are presented as the mean ± SEM

repression of polycomb–target genes in ES cells [53, 54]. Therefore, together with TET1 loss, KDM6B, through its H3K27me3 demethylase activity, could contribute to induce the expression of a subset of these genes upon neural differentiation. Similarly, TET3 could potentiate its genome-wide action by activating *Kdm6b*, as illustrated by the finding that 5hmC gain in the body of active genes is associated with H3K27me3 loss in neurogenesis [39]. The observation that both TET3 and KDM6B belong to the 2-oxoglutarate-dependant dioxygenase enzyme family raises the question of whether their interplay could be a component of a more general program contributing to cellular fitness in response to changes in oxygen levels and/or availability of metabolic co-factors, including iron [55].

Altogether, our observations support the hypothesis that TET3-mediated control of *Kdm6b* expression upon neural commitment could be the central component of a wider epigenetic program whereby 5hmC and H3K27me3 cooperate to control neurogenesis.

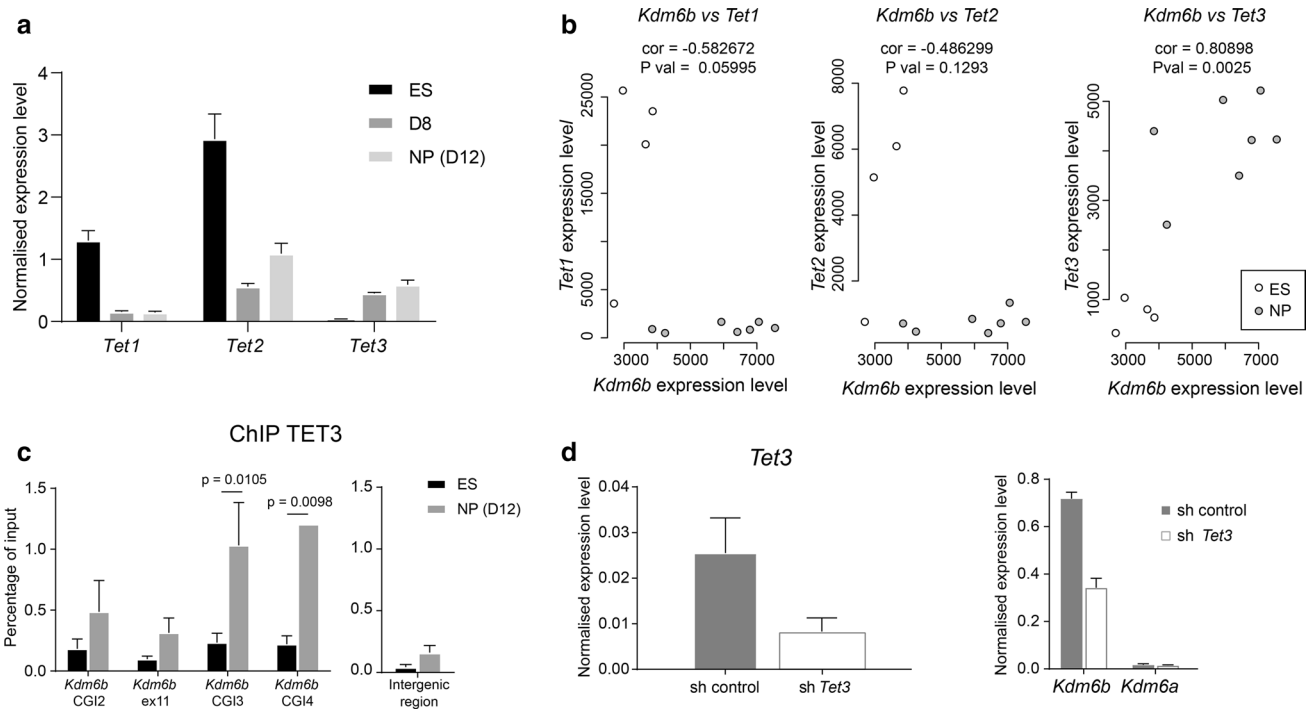

Fig. 4 A role for TET3 in *Kdm6b* upregulation. **a** *Tet1, Tet2,* and *Tet3* expression level at D0 (ES cells) ($n=7$), D8 ($n=5$), and D12 (NP cells) ($n=7$) during in vitro corticogenesis. **b** Correlation analysis of *Kdm6b* and *Tet1* (left panel), *Tet2* (middle panel), and *Tet3* (right panel) expression levels in ES (white dots) and NP cells (gray dots). **c** ChIP analysis of TET3 enrichment at CGI2, exon 11, CGI3, and CGI4 of *Kdm6b* in ES ($n=3$) and NP cells (D12 of in vitro corticogenesis, $n=3$). An intergenic region (chr5:42,282,264–42,282,413 in mm9) was used as negative control. Statistical significance was determined by two-way ANOVA (p values in the figure). The data are presented as the mean ± SEM. **d** The expression level of *Kdm6b* and *Kdm6a* after shRNA-mediated *Tet3* knockdown in NP cells. NP cells that stably integrated a scramble shRNA were used as control (sh control)

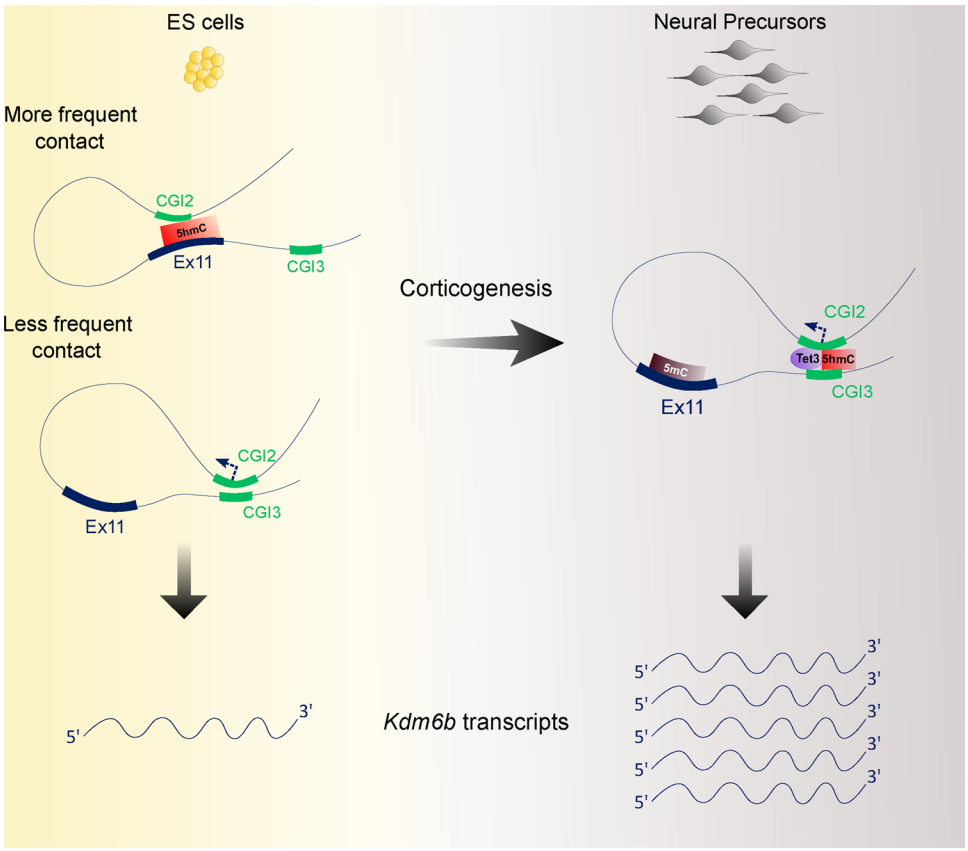

Fig. 5 Model. 5hmC enrichment at exon 11 would favor its unproductive interaction with the *Kdm6b* promoter in ES cells. Productive contacts between CGI2 and CGI3 in a subset of cells would account for the basal *Kdm6b* expression detected at this stage. Upon differentiation, 5mC gain at exon 11 and TET3-mediated 5hmC gain at the CGI3 area would stabilize the CGI2–CGI3 productive interactions and ensure robust *Kdm6b* expression in NP cells

Acknowledgements We thank Claire Chazaud for advice in ES cell derivation and all members of P.A.'s team for critical reading of the manuscript.

Author contributions PA initiated and supervised the study. BM, FC and PA designed the study. BM, JC, TB, AC, SMM, DN, CGG, SC, NA, CCH, CC, IV, CJM, FC and PA performed the experiments. FC performed the bioinformatics analyses. BM, JC, AC, DN, CGG, IV, JM, FC and PA analyzed the data. BM and FC produced the figures with JC's and IV's input. PA wrote the paper. All authors read and approved the final manuscript.

Funding This research has been financed by the French government IDEX-ISITE initiative 16- IDEX-0001 (CAP 20–25) (Emergence, Challenge 3-recherche) (to F. C. and P. A.), the Ligue Contre le Cancer comité de l'Ardéche, du Puy de Dôme and du Cantal (to F. C. and P. A.) and "Conseil Régional d'Auvergne" (to PA). B. M. had a fellowship from Fondation pour la recherche médicale (FRM). C.J.M. is funded by the Portuguese Foundation for Science and Technology (FCT-CEECIND/00371/2017).

References

1. Conway E, Healy E, Bracken AP (2015) PRC2 mediated H3K27 methylations in cellular identity and cancer. Curr Opin Cell Biol 37:42–48. https://doi.org/10.1016/j.ceb.2015.10.003
2. Bernstein BE, Mikkelsen TS, Xie X, Kamal M, Huebert DJ, Cuff J, Fry B, Meissner A, Wernig M, Plath K, Jaenisch R, Wagschal A, Feil R, Schreiber SL, Lander ES (2006) A bivalent chromatin structure marks key developmental genes inembryonic stem cells. Cell 125:315–326
3. Lien WH, Guo X, Polak L, Lawton LN, Young RA, Zheng D, Fuchs E (2011) Genome-wide maps of histone modifications unwind in vivo chromatin states of the hair follicle lineage. Cell Stem Cell 9:219–232. https://doi.org/10.1016/j.stem.2011.07.015
4. Voigt P, Tee WW, Reinberg D (2013) A double take on bivalent promoters. Genes Dev 27:1318–1338. https://doi.org/10.1101/gad.219626.113
5. Azuara V, Perry P, Sauer S, Spivakov M, Jørgensen HF, John RM, Gouti M, Casanova M, Warnes G, Merkenschlager M, Fisher AG (2006) Chromatin signatures of pluripotent cell lines. Nat Cell Biol 8:532–538
6. Barski A, Cuddapah S, Cui K, Roh TY, Schones DE, Wang Z, Wei G, Chepelev I, Zhao K (2007) High-resolution profiling of histone methylations in the human genome. Cell 129:823–837
7. Mikkelsen TS, Ku M, Jaffe DB, Issac B, Lieberman E, Giannoukos G, Alvarez P, Brockman W, Kim TK, Koche RP, Lee W, Mendenhall E, O'Donovan A, Presser A, Russ C, Xie X, Meissner A, Wernig M, Jaenisch R, Nusbaum C, Lander ES, Bernstein BE (2007) Genome wide maps of chromatin state in pluripotent and lineage-committed cells. Nature 448:553–560
8. Pan G, Tian S, Nie J, Yang C, Ruotti V, Wei H, Jonsdottir GA, Stewart R, Thomson JA (2007) Whole-genome analysis of histone H3 lysine 4 and lysine 27 methylation in human embryonic stem cells. Cell Stem Cell 1:299–312
9. Mohn F, Weber M, Rebhan M, Roloff TC, Richter J, Stadler MB, Bibel M, Schübeler D (2008) Lineage-specific polycomb targets and de novo DNA methylation define restriction and potential of neuronal progenitors. Mol Cell 30:755–766. https://doi.org/10.1016/j.molcel.2008.05.007

10. Sanz LA, Chamberlain S, Sabourin JC, Henckel A, Magnuson T, Hugnot JP, Feil R, Arnaud P (2008) A mono-allelic bivalent chromatin domain controls tissue-specific imprinting at Grb10. EMBO J 27:2523–2532. https://doi.org/10.1038/emboj.2008.142
11. Cui K, Zang C, Roh TY, Schones DE, Childs RW, Peng W, Zhao K (2009) Chromatin signatures in multipotent human hematopoietic stem cells indicate the fate of bivalent genes during differentiation. Cell Stem Cell 4:80–93. https://doi.org/10.1016/j.stem.2008.11.011
12. Maupetit-Méhouas S, Montibus B, Nury D, Tayama C, Wassef M, Kota SK, Fogli A, Cerqueira Campos F, Hata K, Feil R, Margueron R, Nakabayashi K, Court F, Arnaud P (2016) Imprinting control regions (ICRs) are marked by mono-allelic bivalent chromatin when transcriptionally inactive. Nucleic Acids Res 44:621–635. https://doi.org/10.1093/nar/gkv960
13. Albert M, Kalebic N, Florio M, Lakshmanaperumal N, Haffner C, Brandl H, Henry I, Huttner WB (2017) Epigenome profiling and editing of neocortical progenitor cells during development. EMBO J 36:2642–2658. https://doi.org/10.15252/embj.201796764
14. Hirabayashi Y, Suzki N, Tsuboi M, Endo TA, Toyoda T, Shinga J, Koseki H, Vidal M, Gotoh Y (2009) Polycomb limits the neurogenic competence of neural precursor cells to promote astrogenic fate transition. Neuron 63:600–613. https://doi.org/10.1016/j.neuron.2009.08.021
15. Pereira JD, Sansom SN, Smith J, Dobenecker MW, Tarakhovsky A, Livesey FJ (2010) Ezh2, the histone methyltransferase of PRC2, regulates the balance between self-renewal and differentiation in the cerebral cortex. Proc Natl Acad Sci USA 107:15957–15962. https://doi.org/10.1073/pnas.1002530107
16. Morimoto-Suzki N, Hirabayashi Y, Tyssowski K, Shinga J, Vidal M, Koseki H, Gotoh Y (2014) The polycomb component Ring1B regulates the timed termination of subcerebral projection neuron production during mouse neocortical development. Development 141(4343):53. https://doi.org/10.1242/dev.112276
17. Yao M, Zhou X, Zhou J, Gong S, Hu G, Li J, Huang K, Lai P, Shi G, Hutchins AP, Sun H, Wang H, Yao H (2018) PCGF5 is required for neural differentiation of embryonic stem cells. Nat Commun 9:1463. https://doi.org/10.1038/s41467-018-03781-0
18. Agger K, Cloos PA, Christensen J, Pasini D, Rose S, Rappsilber J, Issaeva I, Canaani E, Salcini AE, Helin K (2007) UTX and JMJD3 are histone H3K27 demethylases involved in HOX gene regulation and development. Nature 449:731–734
19. De Santa F, Totaro MG, Prosperini E, Notarbartolo S, Testa G, Natoli G (2007) The histone H3 lysine-27 demethylase Jmjd3 links inflammation to inhibition of polycomb-mediated gene silencing. Cell 130:1083–1094
20. Jepsen K, Solum D, Zhou T, McEvilly RJ, Kim HJ, Glass CK, Hermanson O, Rosenfeld MG (2007) SMRT-mediated repression of an H3K27 demethylase in progression from neural stem cell to neuron. Nature 450:415–419
21. Burgold T, Spreafico F, De Santa F, Totaro MG, Prosperini E, Natoli G, Testa G (2008) The histone H3 lysine 27-specific demethylase Jmjd3 is required for neural commitment. PLoS ONE 3:e3034. https://doi.org/10.1371/journal.pone.0003034
22. Burgold T, Voituron N, Caganova M, Tripathi PP, Menuet C, Tusi BK, Spreafico F, Bévengut M, Gestreau C, Buontempo S, Simeone A, Kruidenier L, Natoli G, Casola S, Hilaire G, Testa G (2012) The H3K27 demethylase JMJD3 is required for maintenance of the embryonic respiratory neuronal network, neonatal breathing, and survival. Cell Rep 2:1244–1258. https://doi.org/10.1016/j.celrep.2012.09.013
23. Park DH, Hong SJ, Salinas RD, Liu SJ, Sun SW, Sgualdino J, Testa G, Matzuk MM, Iwamori N, Lim DA (2014) Activation of neuronal gene expression by the JMJD3 demethylase is required for postnatal and adult brain neurogenesis. Cell Rep 8:1290–1299. https://doi.org/10.1016/j.stem.2007.08.003
24. Gaspard N, Bouschet T, Herpoel A, Naeije G, van den Ameele J, Vanderhaeghen P (2009) Generation of cortical neurons from mouse embryonic stem cells. Nat Protoc 4:1454–1463. https://doi.org/10.1038/nprot.2009.157
25. Neely MD, Litt MJ, Tidball AM, Li GG, Aboud AA, Hopkins CR, Chamberlin R, Hong CC, Ess KC, Bowman AB (2012) DMH1, a highly selective small molecule BMP inhibitor promotes neurogenesis of hiPSCs: comparison of PAX6 and SOX1 expression during neural induction. ACS Chem Neurosci 3:482–491. https://doi.org/10.1021/cn300029t
26. Jin SG, Zhang ZM, Dunwell TL, Harter MR, Wu X, Johnson J, Li Z, Liu J, Szabó PE, Lu Q, Xu GL, Song J, Pfeifer GP (2016) Tet3 reads 5-carboxylcytosine through its CXXC domain and is a potential guardian against neurodegeneration. Cell Rep 14:493–505. https://doi.org/10.1016/j.celrep.2015.12.044
27. Arnaud P, Hata K, Kaneda M, Li E, Sasaki H, Feil R, Kelsey G (2006) Stochastic imprinting in the progeny of Dnmt3L−/− females. Hum Mol Genet 15:589–598
28. Santiago M, Antunes C, Guedes M, Iacovino M, Kyba M, Reik W, Sousa N, Pinto L, Branco MR, Marques CJ (2019) Tet3 regulates cellular identity and DNA methylation in neural progenitor cells. Cell Mol Life Sci. https://doi.org/10.1007/s00018-019-03335-7
29. Iacovino M, Bosnakovski D, Fey H, Rux D, Bajwa G, Mahen E, Mitanoska A, Xu Z, Kyba M (2011) Inducible cassette exchange: a rapid and efficient system enabling conditional gene expression in embryonic stem and primary cells. Stem Cells 29:1580–1588
30. Bibel M, Richter J, Lacroix E, Barde YA (2007) Generation of a defined and uniform population of CNS progenitors and neurons from mouse embryonic stem cells. Nat Protoc 2:1034–1043
31. Court F, Baniol M, Hagege H, Petit JS, Lelay-Taha MN, Carbonell F, Weber M, Cathala G, Forne T (2011) Long-range chromatin interactions at the mouse Igf2/H19 locus reveal a novel paternally expressed long non-coding RNA. Nucleic Acids Res 39:5893–5906. https://doi.org/10.1093/nar/gkr209
32. Wagschal A, Delaval K, Pannetier M, Arnaud P, Feil R (2007) Chromatin immunoprecipitation (ChIP) on unfixed chromatin from cells and tissues to analyze histone modifications. Cold Spring Harbor Protocols. https://doi.org/10.1101/pdb.prot4767 **(pdb.prot4767-prot4767)**
33. Bouschet T, Dubois E, Reynès C, Kota SK, Rialle S, Maupetit-Méhouas S, Pezet M, Le Digarcher A, Nidelet S, Demolombe V, Cavelier P, Meusnier C, Maurizy C, Sabatier R, Feil R, Arnaud P, Journot L, Varrault A (2017) In vitro corticogenesis from embryonic stem cells recapitulates the in vivo epigenetic control of imprinted gene expression. Cereb Cortex 27:2418–2433. https://doi.org/10.1093/cercor/bhw102
34. Dixon JR, Selvaraj S, Yue F, Kim A, Li Y, Shen Y, Hu M, Liu JS, Ren B (2012) Topological domains in mammalian genomes identified by analysis of chromatin interactions. Nature 485:376–380. https://doi.org/10.1038/nature11082
35. Bonev B, Mendelson Cohen N, Szabo Q, Fritsch L, Papadopoulos GL, Lubling Y, Xu X, Lv X, Hugnot JP, Tanay A, Cavalli G (2017) Multiscale 3D genome rewiring during mouse neural development. Cell 171:557–572. https://doi.org/10.1016/j.cell.2017.09.043
36. Tahiliani M, Koh KP, Shen Y, Pastor WA, Bandukwala H, Brudno Y, Agarwal S, Iyer LM, Liu DR, Aravind L, Rao A (2009) Conversion of 5-methylcytosine to 5-hydroxymethylcytosine in mammalian DNA by MLL partner TET1. Science 324:930–935. https://doi.org/10.1126/science.1170116
37. Kriaucionis S, Heintz N (2009) The nuclear DNA base 5-hydroxymethylcytosine is present in Purkinje neurons and the brain. Science 324:929–930. https://doi.org/10.1126/science.1169786

38. Sérandour AA, Avner S, Oger F, Bizot M, Percevault F, Lucchetti-Miganeh C, Palierne G, Gheeraert C, Barloy-Hubler F, Péron CL, Madigou T, Durand E, Froguel P, Staels B, Lefebvre P, Métivier R, Eeckhoute J, Salbert G (2012) Dynamic hydroxymethylation of deoxyribonucleic acid marks differentiation-associated enhancers. Nucleic Acids Res 40:8255–8265
39. Hahn MA, Qiu R, Wu X, Li AX, Zhang H, Wang J, Jui J, Jin SG, Jiang Y, Pfeifer GP, Lu Q (2013) Dynamics of 5-hydroxymethylcytosine and chromatin marks in mammalian neurogenesis. Cell Rep 3:291–300. https://doi.org/10.1016/j.celrep.2013.01.011
40. Booth MJ, Branco MR, Ficz G, Oxley D, Krueger F, Reik W, Balasubramanian S (2012) Quantitative sequencing of 5-methylcytosine and 5-hydroxymethylcytosine at single-base resolution. Science 336:934–937. https://doi.org/10.1126/science.1220671
41. Wu H, Zhang Y (2011) Tet1 and 5-hydroxymethylation: a genome-wide view in mouse embryonic stem cells. Cell Cycle 10:2428–2436
42. Greco CM, Kunderfranco P, Rubino M, Larcher V, Carullo P, Anselmo A, Kurz K, Carell T, Angius A, Latronico MV, Papait R, Condorelli G (2016) DNA hydroxymethylation controls cardiomyocyte gene expression in development and hypertrophy. Nat Commun 7:12418. https://doi.org/10.1038/ncomms12418
43. Tsagaratou A, Äijö T, Lio CW, Yue X, Huang Y, Jacobsen SE, Lähdesmäki H, Rao A (2014) Dissecting the dynamic changes of 5-hydroxymethylcytosine in T-cell development and differentiation. Proc Natl Acad Sci USA 111:E3306–E3315. https://doi.org/10.1073/pnas.1412327111
44. Mahé EA, Madigou T, Sérandour AA, Bizot M, Avner S, Chalmel F, Palierne G, Métivier R, Salbert G (2017) Cytosine modifications modulate the chromatin architecture of transcriptional enhancers. Genome Res 27:947–958. https://doi.org/10.1101/gr.211466.116
45. Ren G, Jin W, Cui K, Rodrigez J, Hu G, Zhang Z, Larson DR, Zhao K (2017) CTCF Mediated enhancer–promoter interaction is a critical regulator of cell-to-cell variation of gene expression. Mol Cell 67:1049–1058. https://doi.org/10.1016/j.molcel.2017.08.026
46. Li T, Yang D, Li J, Tang Y, Yang J, Le W (2015) Critical role of Tet3 in neural progenitor cell maintenance and terminal differentiation. Mol Neurobiol 51:142–154. https://doi.org/10.1007/s12035014-8734-5
47. Koh KP, Yabuuchi A, Rao S, Huang Y, Cunniff K, Nardone J, Laiho A, Tahiliani M, Sommer CA, Mostoslavsky G, Lahesmaa R, Orkin SH, Rodig SJ, Daley GQ, Rao A (2011) Tet1 and Tet2 regulate 5-hydroxymethylcytosine production and cell lineage specification in mouse embryonic stem cells. Cell Stem Cell 8:200–213. https://doi.org/10.1016/j.stem.2011.01.008
48. Dawlaty MM, Ganz K, Powell BE, Hu YC, Markoulaki S, Cheng AW, Gao Q, Kim J, Choi SW, Page DC, Jaenisch R (2011) Tet1 is dispensable for maintaining pluripotency and its loss is compatible with embryonic and postnatal development. Cell Stem Cell 9:166–175. https://doi.org/10.1016/j.stem.2011.07.010
49. Williams K, Christensen J, Pedersen MT, Johansen JV, Cloos PA, Rappsilber J, Helin K (2011) TET1 and hydroxymethylcytosine in transcription and DNA methylation fidelity. Nature 473:343–348. https://doi.org/10.1038/nature10066
50. Dawlaty MM, Breiling A, Le T, Raddatz G, Barrasa MI, Cheng AW, Gao Q, Powell BE, Li Z, Xu M, Faull KF, Lyko F, Jaenisch R (2013) Combined deficiency of Tet1 and Tet2 causes epigenetic abnormalities but is compatible with postnatal development. Dev Cell 24:310–323. https://doi.org/10.1016/j.devcel.2012.12.015
51. Reimer M Jr, Pulakanti K, Shi L, Abel A, Liang M, Malarkannan S, Rao S (2019) Deletion of Tet proteins results in quantitative disparities during ESC differentiation partially attributable to alterations in gene expression. BMC Dev Biol 19:16. https://doi.org/10.1186/s12861-019-0196-6
52. Dawlaty MM, Breiling A, Le T, Barrasa MI, Raddatz G, Gao Q, Powell BE, Cheng AW, Faull KF, Lyko F, Jaenisch R (2014) Loss of Tet enzymes compromises proper differentiation of embryonic stem cells. Dev Cell 29:102–111. https://doi.org/10.1016/j.devcel.2014.03.003
53. Wu H, D'Alessio AC, Ito S, Xia K, Wang Z, Cui K, Zhao K, Sun YE, Zhang Y (2011) Dual functions of Tet1 in transcriptional regulation in mouse embryonic stem cells. Nature 473:389–393. https://doi.org/10.1038/nature09934
54. Wu H, D'Alessio AC, Ito S, Wang Z, Cui K, Zhao K, Sun YE, Zhang Y (2011) Genome wide analysis of 5-hydroxymethylcytosine distribution reveals its dual function in transcriptional regulation in mouse embryonic stem cells. Genes Dev 25:679–684. https://doi.org/10.1101/gad.2036011
55. Karuppagounder SS, Kumar A, Shao DS, Zille M, Bourassa MW, Caulfield JT, Alim I, Ratan RR (2015) Metabolism and epigenetics in the nervous system: creating cellular fitness and resistance to neuronal death in neurological conditions via modulation of oxygen-, iron-, and 2-oxoglutarate-dependent dioxygenases. Brain Res 1628(Pt B):273–287. https://doi.org/10.1016/j.brainres.2015.07.030